Journal of the Optical Society of America B

OPTICAL PHYSICS

Optical waveguiding by necklace and azimuthon beams in nonlinear media

L. Stoyanov,[1] N. Dimitrov,[1] I. Stefanov,[1] D. N. Neshev,[2] and A. Dreischuh[1,*]

[1]Faculty of Physics, Department of Quantum Electronics, Sofia University, 5, J. Bourchier Blvd., Sofia-1164, Bulgaria
[2]Nonlinear Physics Centre, Research School of Physics and Engineering, The Australian National University, Canberra, 2601 ACT, Australia
*Corresponding author: ald@phys.uni-sofia.bg

Received 1 December 2016; revised 19 February 2017; accepted 20 February 2017; posted 21 February 2017 (Doc. ID 282046); published 13 March 2017

Nonlinear necklace and azimuthon beams were experimentally generated in a self-focusing bulk photorefractive nonlinear medium (crystal SBN:60) using a frequency-doubled Nd:YVO_4 laser at 532 nm. The parallel optical waveguides induced by such a beam were probed by near-infrared signal beams emitted by a Ti:Sapphire laser. The quality and time stability of the guided sub-beams at the exit of the crystal were investigated. In view of the waveguides' ordering along a ring, the best matching probe beams were found to be singly or doubly charged optical vortex bright rings. The results indicate the feasibility of parallel all-optical guiding of optical signals at wavelengths, for which the nonlinear medium is not photosensitive.

OCIS codes: (050.4865) Optical vortices; (090.1760) Computer holography; (190.4420) Nonlinear optics, transverse effects in; (190.5330) Photorefractive optics; (190.5940) Self-action effects; (230.1150) All-optical devices.

https://doi.org/10.1364/JOSAB.34.000801

1. INTRODUCTION

Spatial optical solitons [1,2]—stationary self-trapped localized beams in third-order nonlinear media—belong to the most intensively studied nonlinear objects. As early as in the first analysis, the authors formulated the concept of all-optical waveguiding [1], which stimulated intensive research: because the beam, once trapped, establishes a waveguide of appropriate characteristics for its own conduction, weak waves can be conducted [1]. As is known, optical solitons in media with an instantaneous isotropic self-focusing nonlinearity are unstable due to the critical collapse at high powers [3–6]. In a local saturable self-focusing nonlinear medium (NLM), however, one observes robust self-trapping of optical vortex beams over several Rayleigh diffraction lengths [7].

In the context of bright optical beams, the soliton cluster has been introduced in [8,9] as a multi-soliton bound state in a homogeneous bulk optical NLM. Its rich transverse dynamics [10] can be intuitively understood recalling that, depending on their relative soliton phase $\delta\vartheta$, in general, two spatial solitons attract for $\delta\vartheta = 0$ or repel each other for $\delta\vartheta = \pi$ [11]. Similarly, considering $\delta\vartheta$ as the magnitude of the phase jump between two solitons of the cluster, when $0 < \delta\vartheta < \pi/2$, the interaction between solitons is attractive, whereas for $\pi/2 < \delta\vartheta < \pi$ it is a repulsive one. In the particular case $\delta\vartheta = \pi$, as shown in Fig. 1(a), the cluster expands without rotation as a necklace-type beam [8,12]. The intensity of the necklace beam is periodically modulated azimuthally and the adjacent bright sub-beams on the ring differ in phase by π [Fig. 1(a)]. The necklace beam is predicted to be stable in nonlinear media for $(2 + 1)$ spatial dimensions when the azimuthal period of the ring (the sub-beam-to-sub-beam distance) is much smaller than the ring radius (i.e., the ring curvature vanishes). The necklace-ring beams expand slowly but fully preserve their structure [8]. More precisely, the analyses have shown [13] that the incoherent interaction between the components of a vector ring-like beam allows one to compensate for the coherent repulsion of the sub-beams, so that stationary self-trapped necklace-ring vector solitons can be formed. A comprehensive overview of the early results on necklace beams and ring-like soliton clusters can be found in [14]. The concept of multipole vector spatial solitons formed by the interaction of co-propagating, mutually incoherent optical beams in a saturable bulk NLM has been presented in detail in [15].

The *azimuthons* were introduced for the first time in [16] as spatially localized self-trapped ring-like singular optical beams [Fig. 1(b)] in NLM. They appear due to a continuous azimuthal deformation of vortex solitons and, in contrast with the necklace beam, carry a net angular momentum. As opposed to the linear vortex phase $m\varphi$ [see Fig. 1(c)], where m is the vortex topological charge (TC) and φ is the polar angle, the phase of the azimuthon is a staircase-like nonlinear function of φ [16], as shown in Fig. 1(b). The azimuthon family includes clusters with negative, positive, and zero angular velocity, defined by the phase inclination α, as indicated in Fig. 1(b).

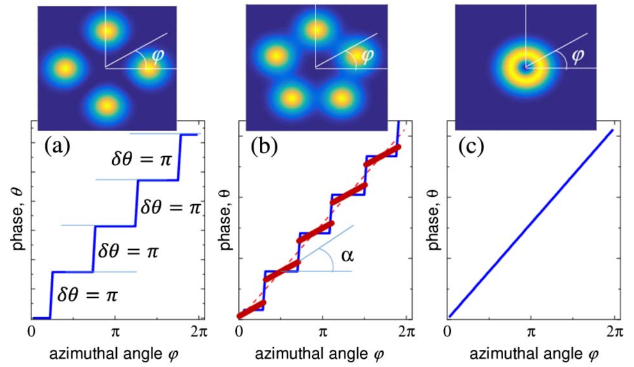

Fig. 1. Intensity (top) and phase (bottom) structure of different types of spatial soliton beams: (a) four-lobe necklace type beams; (b) five-lobe azimuthon beam. The general phase shape can feature a non-zero phase-tilt across each lobe. (c) Vortex-type beam.

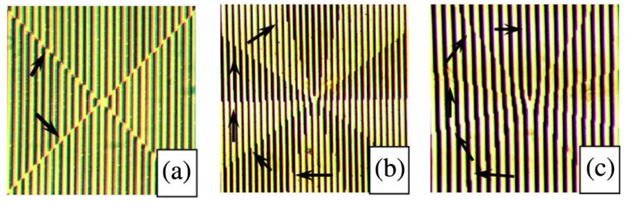

Fig. 2. Computer-generated holograms of (a) a quasi-2D dark beam, of (b) an OV with TC = 1 and grating period of 20 μm, and, again, of (c) a singly charged OV with a grating period of 30 μm. The areas of azimuthal modulations are depicted by rotated arrows to remind the reader of the OV helical phase profiles.

The rotation can be suppressed by a uniform energy flow along the ring; the azimuthon then remains stationary [16].

The first experimental generation of optical azimuthons utilized picosecond laser pulses in a Kerr nonlinear medium, demonstrating azimuthons of order 3 and 13, having a trivial phase profile [17]. Later, [18] reported on the observation of optical azimuthons with three and four lobes and a complex phase profile, generated by phase imprinting in hot Rb vapors. It was shown that the presence of azimuthal intensity and phase modulation leads to spatial rotation of the azimuthon in the self-focusing NLM [18], where the nonlinear interaction of azimuthon lobes slows down and even inverts the direction of rotation. Furthermore, [19] showed that even a Bose–Einstein condensate trapped by an annular potential induced by a Laguerre–Gaussian pump supports azimuthons. In this physical system, azimuthons can form spontaneously due to the presence of thermal noise. Finally, the formation of self-trapped dipole azimuthons has been demonstrated in nematic liquid crystals [20], as being due to these crystals' re-orientational nonlinearity.

Despite such general interest in optical necklace beams and azimuthons in particular, their guiding properties have not been the subject of thorough studies. To the best of our knowledge, we present here, for the first time to the best of our knowledge, a study on the waveguiding properties of optical necklace and azimuthon beams in a photorefractive nonlinear medium at 532 nm. We show that, as a consequence of their self-focusing, such beams can guide other strong beams at non-photosensitive wavelengths.

2. EXPERIMENTAL SETUP

Four-lobe necklace beams and azimuthon beams were generated in the following way: we let the input Gaussian beam diffract in the first diffraction order from a computer-generated hologram (CGH) of a quasi-2D dark beam [see Fig. 2(a)] or in second/fifth diffraction order of the CGHs of optical vortices (OVs), as shown in Figs. 2(b) and 2(c), respectively. Thus, in the second diffraction order of the CGH, as shown in Fig. 2(b), we obtained a linear azimuthon beam with five bright lobes. Alternatively, in the fifth diffraction order of the CGH in Fig. 2(c), we obtained a linear azimuthon with 10 lobes. From the CGH of the quasi-2D dark beam [Fig. 2(a)], we produced four bright subpeaks of a necklace beam. Self-focusing was initiated in a photorefractive SBN:60 crystal. The CGHs of the singular beams used were of a binary type, produced photolithographically with a grating period of 20 μm [Figs. 2(a) and 2(b)] and 30 μm [Fig. 2(c)]. Due to their binary nature and the necessity to have curved reflecting stripes consisting of two pixels of 5 μm width for the 20 μm grating and 3 pixels of 5 μm width for the 30 μm grating, in some areas 1 pixel disappears on one side of the stripe appearing farther on its opposite side. As a result, on the holograms of the vortices we observed a specific azimuthal modulation of the grating transmission/reflection [see the microscope photographs shown in Figs. 2(b) and 2(c)]. This modulation, however, results in a phase modulation of the diffracted beams and is multiplied by the diffraction order. In this way, bright azimuthon sub-beams surrounding the OV core were reproducibly experimentally generated, well separated by dark radial stripes. In the case of a necklace structure with four peaks, the hologram used [see Fig. 2(a)] splits the input Gaussian beam in four sub-peaks due to the encoded crossed 1D (diagonal) phase jumps by π. The experimental setup (Fig. 3) involved a green pump beam from a frequency-doubled continuous-wave Nd:YVO_4 laser carrying the desired phase singularities and the surrounding ring-like ordered bright sub-beams, which further self-focus in the SBN crystal. The probe beam used for testing the properties of the induced waveguides and their time stability was a near-infrared continuous-wave beam emitted from a Ti:Sapphire laser. For diagnostic purposes, the beam of the green laser was split by a beam splitter (BS) and, later, the object and the reference beams were recombined by a second BS to interfere at the CCD camera chip. Behind the CGHs, the desired diffraction order beam was selected by an iris diaphragm D and focused by a lens FL on the front facet of a 6 mm long SBN:60 photorefractive crystal of a cross-section 6 mm × 10 mm. The laser beam polarization was parallel to the crystalline c axis; thus the beam experienced strong photorefractive nonlinearity due to the high electro-optic coefficient r_{33} in the SBN. The crystal was biased by an electric field E_0 ranging from 600 V/cm to 700 V/cm. The front or back facet of the crystal was imaged by a lens IL onto a charge-coupled device (CCD) camera, both moving on translation stages. Power density distributions of the resulting optical beams and the respective interference patterns were recorded by the same CCD camera by

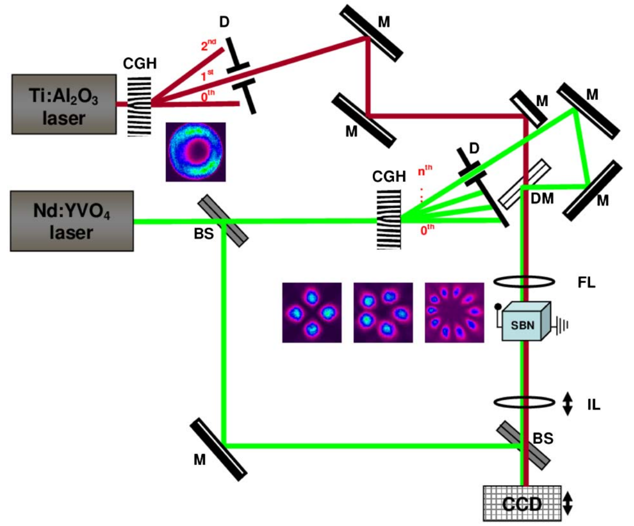

Fig. 3. Experimental setup. Nd:YVO_4, continuous-wave frequency-doubled laser emitting at a wavelength $\lambda = 532$ nm; Ti:Al_2O_3, titanium-sapphire continuous-wave laser generating the probe beam at $\lambda = 808$ nm. BS, beam splitters; DM, dichroic mirror; CGH, binary computer-generated holograms; D, diaphragms; FL, focusing lens ($f = 3.5$ cm); M, flat silver mirrors; SBN, photorefractive crystal; IL and CCD, imaging lens and charge-coupled device (CCD) camera, both moving on a translation stages, imaging the front or the exit facet of the SBN crystal.

blocking/unblocking the reference laser beam, while keeping the camera position unchanged. Special attention was paid to the CGHs alignment in order to place the dark singular beams well centered with respect to the illuminating beam. The power of the background beam was adjusted so as to initiate weak beam self-focusing only. We refrained from further increasing the background beam power to avoid filamentation in the crystal. In this way we created optically induced waveguides in the photorefractive NLM.

The probe beam in this setup was the output beam of a Ti:Sapphire continuous-wave laser operated at a wavelength of 808 nm. We first used the direct-output Gaussian beam as a probe beam, but this resulted in a dominating central peak, and the induced waveguiding was not well seen. In order to obtain better spatial matching of the probe wave with the necklace and azimuthon guiding structures in the bulk SBN crystal, we changed the beam profile to a Laguerre–Gaussian one generating an optical vortex beam (OV) with a single or double charge. For this purpose, in the probe arm of the setup, we placed another CGH encoded with an OV of the desired TC. The first diffraction order beam was selected by a diaphragm and then matched to the previously induced waveguides in the SBN crystal.

3. RESULTS AND DISCUSSION

Regardless of the number of bright lobes in the necklace and in the azimuthon structure, all measurements presented here refer to a mean power of the green laser of 110 μW measured before the focusing lens. The crystal illumination time was 5 min, and the electric field applied on the SBN crystal was $650\ V/\mathrm{cm}$.

In Table 1 we show the measured values of the total (peak-to-peak) width of the structures on the front facet of the SBN crystal, on its exit facet after linear diffraction, and the size of these beams on the exit facet after the nonlinear process of self-focusing has been initiated. Data also are shown for the sizes of the individual lower (or lower left) single peak for each of these bright structures. In these notations, x is the horizontal Cartesian coordinate system axis, y is the vertical one. These measured beam sizes (see Table 1) are strong evidence for the clear experimental discrimination between linear propagation (2D diffraction) and the initial stage of nonlinear self-focusing. Bearing this in mind, we can conclude that, in the regime used, the nonlinearity clearly dominates over the diffraction, and the induction of the parallel waveguides in the crystal is a result of a nonlinear interaction. We also measured the angular spreading of the generated azimuthons. The data show that the linear divergence of the azimuthon with five lobes is 16 mrad, whereas for the azimuthon with 10 lobes it increases to 24 mrad. In the nonlinear case, the divergence of the five-lobe structure increases from 16 to 18 mrad still remaining smaller as compared with this for the 10-lobe structure—20 mrad. These data are accurate to within ± 1 mrad. Our estimations also indicated that the necklace beam experiences linear and nonlinear divergences of 15 and 17 mrad, respectively, accurate to within ± 0.7 mrad. In Fig. 4 we present gray-scale images of the recorded power density distributions of the input necklace (upper left-hand frame) and the input azimuthons (upper middle and right-hand frames) and the respective data on the exit facet of the crystal after linear diffraction (middle row) and after the nonlinear process of self-focusing (lower row). All recorded frames are

Table 1. Comparison between the Width of the Necklace Beam with Four Sub-beams and of the Vortex Azimuthon Beams with 5 and 10 Lobes on the Front Facet of the Crystal, on the Exit Facet in the Linear Regime of Propagation and, on the Exit Facet, but After the Nonlinear Process of Self-focusing has been Initiated[a]

	On the Front Facet of the Crystal			On the Back Facet After Linear Diffraction			On the Back Facet After Self-Focusing		
		Single Peak Size [μm]			Single Peak Size [μm]			Single Peak Size [μm]	
Number of Peaks	Width [μm]	x_{in}	y_{in}	Width [μm]	x_{out}	y_{out}	Width [μm]	x_{out}	y_{out}
4	553	164	200	729	211	300	753	100	170
5	544	199	204	745	254	260	762	160	170
10	771	124	191	1064	160	240	1013	80	160

[a]The sizes of a single lower/lower left peak from these structures in the same three cases (see Fig. 4) are shown, too.

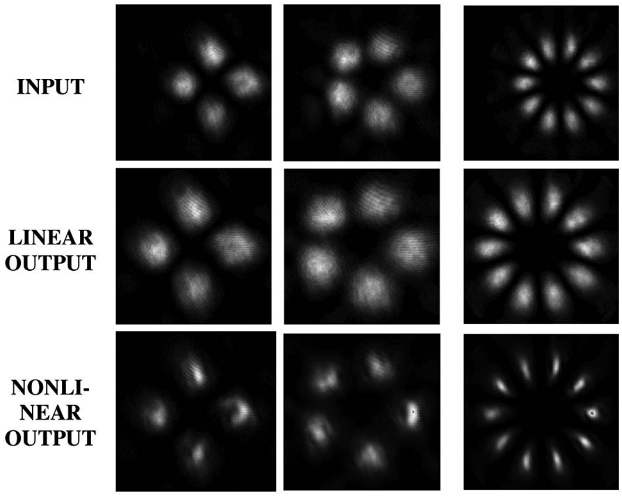

Fig. 4. Power density distributions of the necklace beam (left-hand column) and of the azimuthons (middle and right-hand columns) on the input (upper row) and on the exit of the crystal after *linear diffraction* (middle) and *after nonlinear self-focusing* (lower row).

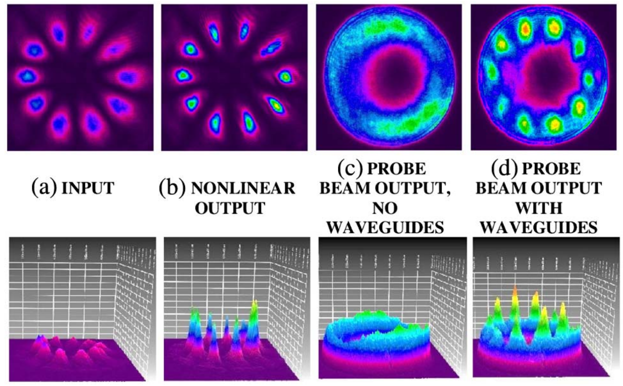

Fig. 6. Initial stage of self-focusing of a vortex azimuthon beam with 10 lobes and central OV generated from a CGH encoded with an OV with TC = 1 in the fifth diffraction order. Upper row: power density distribution of the pump azimuthon beam on the exit facet (a) after linear propagation and (b) after self-focusing, as well as (c) probe beam profile on the exit facet of the SBN crystal without induced waveguides and (d) after illuminating the inscribed ring-like ordered waveguides. Lower row: the same four cases in a 3D representation for better visibility.

directly comparable in size because the CCD camera positions were reproducible.

In Fig. 5 we show experimental evidence of the nonlinear phase structure of the generated azimuthons in the particular case of a 10-lobe structure. In the nonlinear regime shown in the right-hand column in this figure, the sub-beam's peak intensity is approximately three times higher as compared with the linear case. At the maximum 3.5 times increase of the peak lobe intensity in this measurement (not shown), the results were qualitatively similar: Even at a nonlinearly accelerated broadening of the radial dark beams, the interference half-rings between the azimuthon lobes, especially the inner 3–4 interference arcs, remain clearly offset in the radial direction (see the arrows in Fig. 5). Hence, the typical azimuthal staircase-like phase structure of the azimuthons [see Fig. 1(b)] survives the initial stage of its weak self-focusing.

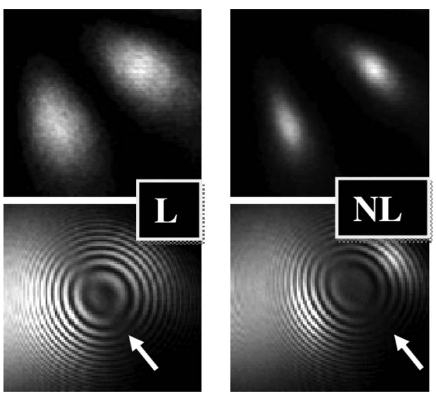

Fig. 5. Selected portion of the power density distribution of the 10-lobe azimuthon beam (upper row) and interference pattern recorded covering two neighboring sub-beams with a reference spherical wave (lower row) in linear and nonlinear regimes (left-hand and right-hand column, respectively). Some 20% of the recorded beam's cross-section are shown. Arrows (directions) along which the interference arcs are offset.

With the setup shown in Fig. 3, we studied every single case separately. In addition to the weak self-focusing of the bright sub-beams and the inscription of waveguides, we also examined the guiding of a probe beam in these parallel guiding structures.

The first experimental set of data shown in Fig. 6 concerns the case of a bright azimuthon with 10 lobes and a central optical vortex with a TC = 5. This azimuthon was created by a CGH [Fig. 2(c)] of an OV with a TC = 1 diffracted from the CGH in the fifth diffraction order. The highest efficiency in the first diffraction order of the binary CGHs we used was typically close to the 10% limit predicted [21] and decreased drastically as the diffraction order was increased. In view of the relatively high laser power required in front of the CGH, this was the most difficult case to study experimentally in this work. (Of course, reflective liquid-crystal phase modulators can improve this situation.) We managed to nonlinearly achieve a relative increase of the beam's intensity from about four times for the least self-focused lobe up to six times for the most strongly focused lobe. The 808 nm probe beam was an optical vortex ring carrying an OV with a TC = 2. The input (a) and the self-focused output azimuthon structure (b) are shown in the two left-hand columns in Fig. 6, respectively, whereas the exit probe beam (c) without and (d) with inscribed waveguides is shown in the two right-hand columns of the same figure.

The applied electric field was parallel to the crystalline c axis; thus, the nonlinearity slightly dominated along the horizontal (x) direction across the azimuthon beam. This can be seen in Fig. 6(b), upper row, and (somewhat better) in the 3D view of the same distribution. As seen, the strongest self-focused bright lobes are located along the horizontal (x) axis, while along the perpendicular (y) axis the process is relatively weaker. In the two right-hand columns with experimental frames in Fig. 6, one can see the exit probe beam profile at no inscribed waveguiding structure (c) and its reshaping after passing through the optically induced ring-like ordered waveguides.

The continuous-wave probe beam emitted by the Ti:Al_2O_3 laser ($\lambda = 808$ nm) passed through a CGH of an OV with a TC = 2. The singular probe beam created in this way was used in a cw mode, although generation of OVs in the broad-bandwidth fields of femtosecond mode-locked lasers is a solved problem [22–25]. As seen in Fig. 6(d), all inscribed waveguides are well illuminated by this probe beam, and the guided peaks appear clearly visible and well-formed. The obvious stronger guided peaks along the vertical (y) direction [see Fig. 6(d)] are unfortunately due to the non-perfect azimuthal structure of the probe vortex beam [see Fig. 6(c)].

Further, we studied the transformation and self-focusing of the azimuthon with five lobes and a central charge-two OV. This structure was generated by another CGH of an OV with TC = 1 and a grating period of 20 μm [Fig. 2(b); see the specific azimuthal modulations, which lead to a decay of the bright ring into five sub-peaks] but this time in the second diffraction order. In this case, the main problem, except for the low efficiency in the second (and each even) diffraction order of the binary hologram, was the slight overlapping of the single peaks. This is due to the fact that the phase jump between each two neighboring peaks was less than π ($(4/5)\pi$ according to our estimation). The experimental data and the recorded frames for this case can be seen in Fig. 7.

One can see once again the domination of the self-focusing along the nonlinear crystal's c axis [Fig. 7(b)] and the stronger self-focusing of the peaks along this direction. As in the previous case, the probe beam profile is Laguerre–Gaussian, but this time the vortex is carrying a TC = 1. As a result, as needed, the input bright vortex ring has a smaller diameter. As seen in Fig. 7(d), all waveguides induced are clearly visible and well-formed when illuminated by the infrared probe beam. The different power density distributions of the probe beams in some of the induced waveguides are, unfortunately, again due to the azimuthal irregularity of the probe OV beam's intensity profile.

The last case that we will discuss here is the self-focusing of a necklace beam with four sub-peaks generated by reproducing a CGH of a quasi-2D dark beam with π phase jumps between each quadrant [see Fig. 2(a)]. After optically inscribing four waveguides in the SBN crystal, the guiding properties of the structure were examined by probe beams with two different (Gaussian and Laguerre–Gaussian) profiles. The experimental results are summarized in Fig. 8. In this case, in addition to the ring-shaped probe beam carrying an OV, we show, for comparison, waveguiding with a Gaussian probe beam. As mentioned, the infrared beam ($\lambda = 808$ nm) was emitted by the Ti:Al_2O_3 laser. This time the laser oscillator was mode-locked and emitted sub-30-fs pulses at a repetition rate of some 80 MHz. The aim of this measurement was to show that femtosecond lasers pulses can propagate in the induced waveguides for several minutes without erasing them, provided they are emitted at a wavelength for which the photorefractive crystal has weak photosensitivity. The Gaussian femtosecond probe beam illuminating the induced waveguides is shown in Fig. 8(c). In the lower row of Fig. 8(c), we slightly tilted the experimental frame in order to obtain better visibility of the probe beam on the exit facet of the crystal. As seen, the portions of the guided probe beam appear as four peaks with nearly the same intensities located in the wings of the Gaussian beam. In this case, the central peak of the input Gaussian probe wave remains nearly unaffected by the guiding and is strongly dominating over the guided peaks. This was why we preferred to use vortex rings of different radii (i.e., Laguerre–Gaussian beams) for the measurements presented in Figs. 5 and 6. In the present case of a four-peaked input necklace structure, we also show such data-inscribed waveguides [Fig. 8(b)] illuminated by a vortex probe beam generated from a CGH of an OV with TC = 1 [Fig. 8(d)]. As in the previous two experimental cases reported here, we see a clear waveguiding effect, unfortunately with different exit peak powers of the guided probe beams due to an unwanted irregularity of the vortex ring's intensity profile on the entrance of the crystal.

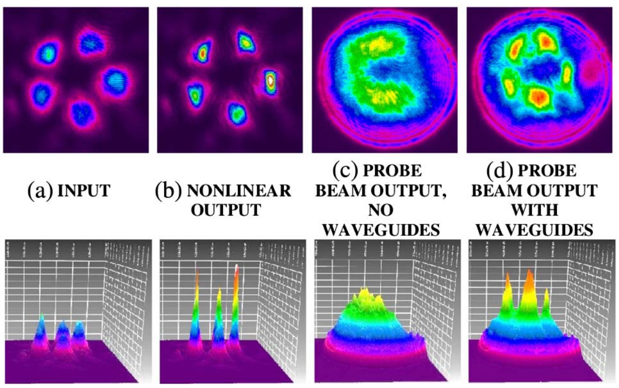

Fig. 7. Initial stage of self-focusing of an azimuthon beam with five lobes generated from a CGH of an OV with TC = 1 in second diffraction order. Upper row: power density distribution of the pump beam on the exit facet (a) after linear propagation and (b) after the process of self-focusing as well as (c) probe beam profile on exit facet of the SBN crystal without induced waveguides and (d) after illuminating the inscribed ring-like ordered waveguides. Lower row: the same four cases in a 3D representation for better visibility.

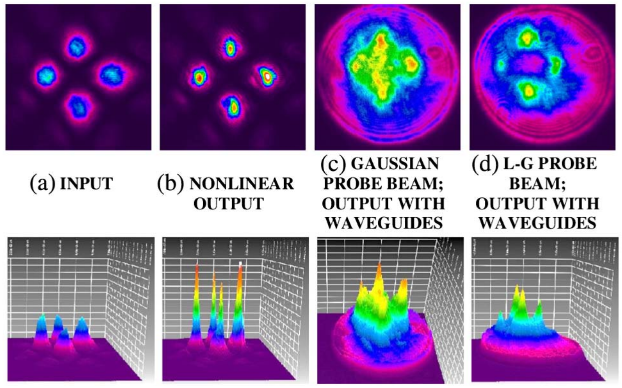

Fig. 8. Initial stage of self-focusing of a necklace with four sub-peaks generated from a CGH of a quasi-2D dark beam in first diffraction order. Upper row: power density distributions of the pump beam on the exit facet (a) after linear propagation and (b) after the process of self-focusing as well as (c) Gaussian and Laguerre–Gaussian probe beam profile (OV with TC = 1) on the (d) exit facet of the SBN after illuminating the inscribed waveguides. Lower row: the same four cases in a 3D representation for better visibility.

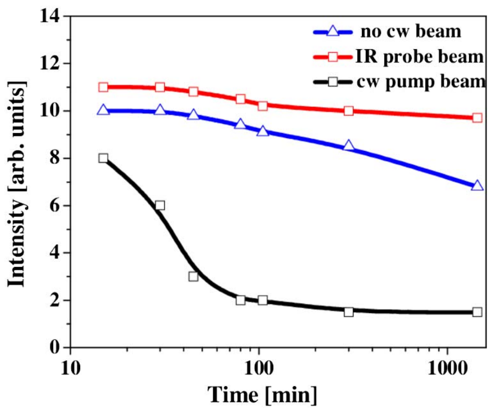

Fig. 9. Stability of the optically induced waveguides versus time probed continuously by a green cw laser beam (black squares/line; 532 nm), by the same green laser operated periodically for a few seconds after large time intervals (blue triangles/line) and by a near-infrared laser beam operated in the same periodical manner (red squares/line).

Using probe beams, we also examined the time stability of the inscribed waveguiding structures in the SBN crystal with both green probe cw emission (532 nm) and femtosecond laser pulses (at the spectrum central wavelength of 808 nm). The results from these measurements are summarized in the graph shown in Fig. 9. We studied experimentally three cases. In the first case, we illuminated the crystal by the green Gaussian cw laser beam (532 nm), with no electric field biasing the crystal. As one can expect, because the SBN crystals are highly photosensitive in the green spectral range, the beam, which initially induced the waveguides, is now erasing them. In the second case, we illuminated the crystal for a few seconds after large time intervals. Even for such short illumination time, the waveguides started decaying. Generally, the waveguides showed good stability for longer than 24 h. The slight decline of the curve is due to the wavelength used of 532 nm. In the third case, we illuminated the inscribed waveguides by a probe beam from a mode-locked Ti:Sapphire laser ($\lambda = 808$ nm). As one can see from the graph in Fig. 9, the waveguides remain remarkably stable even after 24 h.

4. CONCLUSION

The experimental data presented show that periodical azimuthal modulation in the reflecting/transmitting stripes of binary computer-generated holograms can lead to a controllable vortex decay into azimuthon beams with an adjustable number of out-of-phase bright lobes. The nonlinearly accelerated defocusing of the central vortex is able to contribute to the initiation of a controllable self-focusing of the bright sub-beams. The results obtained indicate that parallel all-optical guiding of optical signals at wavelengths, for which the medium (a photorefractive crystal) is not photosensitive, is feasible in azimuthon lobes and necklace peaks.

Funding. National Science Fund (Bulgaria) (DFNI-T-02/10).

Acknowledgment. The studies are carried out in the framework of the Erasmus Mundus NANOPHI project, contract number 2013-5659/002-001. The participation of L. Stoyanov and N. Dimitrov was supported by Operational Programme Human Resource Development 2007–2013 of the European Union, project no. BG051 PO001-3.3.06-0057. A. D. dedicates his work in loving memory to his mother Mrs. Leonora Dreischuh who passed away so unexpectedly.

REFERENCES

1. R. Chiao, E. Garmire, and C. H. Townes, "Self-trapping of optical beams," Phys. Rev. Lett. **13**, 479–482 (1964).
2. Y. S. Kivshar and G. P. Agrawal, *Optical Solitons: From Fibers to Photonic Crystals* (Academic, 2003).
3. V. Tikhonenko, J. Christou, and B. Luther-Davies, "Spiraling bright spatial solitons formed by the breakup of an optical vortex in a saturable self-focusing medium," J. Opt. Soc. Am. B **12**, 2046–2052 (1995).
4. V. Tikhonenko, J. Christou, and B. Luther-Davies, "Three dimensional bright spatial soliton collision and fusion in a saturable nonlinear medium," Phys. Rev. Lett. **76**, 2698–2701 (1996).
5. W. J. Firth and D. V. Skryabin, "Optical solitons carrying orbital angular momentum," Phys. Rev. Lett. **79**, 2450–2453 (1997).
6. D. V. Skryabin and W. J. Firth, "Dynamics of self-trapped beams with phase dislocation in saturable Kerr and quadratic nonlinear media," Phys. Rev. E **58**, 3916–3930 (1998).
7. A. S. Reyna, G. Boudebs, B. A. Malomed, and C. B. de Araujo, "Robust self-trapping of vortex beams in a saturable optical medium," Phys. Rev. A **93**, 013840 (2016).
8. M. Soljacic, S. Sears, and M. Segev, "Self-trapping of necklace beams in self-focusing Kerr media," Phys. Rev. Lett. **81**, 4851–4854 (1998).
9. A. S. Desyatnikov and Y. S. Kivshar, "Rotating optical soliton clusters," Phys. Rev. Lett. **88**, 053901 (2002).
10. A. Desyatnikov, C. Denz, and Y. Kivshar, "Nonlinear optical beams carrying phase dislocations," J. Opt. A **6**, S209–S212 (2004).
11. G. I. Stegeman and M. Segev, "Optical spatial solitons and their interactions: universality and diversity," Science **286**, 1518–1523 (1999).
12. M. Soljacic and M. Segev, "Integer and fractional angular momentum borne on self-trapped necklace-ring beams," Phys. Rev. Lett. **86**, 420–423 (2001).
13. A. S. Desyatnikov and Y. S. Kivshar, "Necklace-ring vector solitons," Phys. Rev. Lett. **87**, 033901 (2001).
14. A. S. Desyatnikov and Y. S. Kivshar, "Spatial optical solitons and soliton clusters carrying an angular momentum," J. Opt. B **4**, S58–S65 (2002).
15. A. S. Desyatnikov, D. N. Neshev, E. A. Ostrovskaya, Y. S. Kivshar, G. McCarthy, W. Krolikowski, and B. Luther-Davies, "Multipole composite spatial solitons: theory and experiment," J. Opt. Soc. Am. B **19**, 586–595 (2002).
16. A. S. Desyatnikov, A. A. Sukhorukov, and Y. S. Kivshar, "Azimuthons: spatially modulated vortex solitons," Phys. Rev. Lett. **95**, 203904 (2005).
17. A. Barthelemy, C. Froehly, and M. Shalaby, "Nonlinear propagation of picoseconds tubular beams: self phase modulation and induced refraction," Proc. SPIE **2041**, 104–113 (1994).
18. A. Minovich, D. N. Neshev, A. S. Desyatnikov, W. Krolikowski, and Y. S. Kivshar, "Observation of optical azimuthons," Opt. Express **17**, 23610–23616 (2009).
19. G. Li, "Azimuthons and pattern formation in annularly confined exciton-polariton Bose-Einstein condensates," Phys. Rev. A **93**, 013837 (2016).
20. Y. V. Izdebskaya, A. S. Desyatnikov, G. Assanto, and Y. S. Kivshar, "Dipole azimuthons and vortex charge flipping in nematic liquid crystals," Opt. Express **19**, 21457–21466 (2011).
21. W.-H. Lee, "Computer-generated holograms: techniques and applications," Prog. Opt. **16**, 119–232 (1978).

22. K. Bezuhanov, A. Dreischuh, G. G. Paulus, M. G. Schätzel, and H. Walther, “Vortices in femtosecond laser fields,” Opt. Lett. **29**, 1942–1944 (2004).
23. I. G. Mariyenko, J. Strohaber, and C. J. G. J. Uiterwaal, “Creation of optical vortices in femtosecond pulses,” Opt. Express **13**, 7599–7608 (2005).
24. G. A. Swartzlander, “Achromatic optical vortex lens,” Opt. Lett. **31**, 2042–2044 (2006).
25. I. Zeylikovich, H. I. Sztul, V. Kartazaev, T. Le, and R. R. Alfano, “Ultrashort Laguerre–Gaussian pulses with angular and group velocity dispersion compensation,” Opt. Lett. **32**, 2025–2027 (2007).